

AD-A095 706

ARIZONA UNIV TUCSON OPTICAL SCIENCES CENTER F/G 20/5
STUDY OF CHEMICAL REACTIONS AND ENERGY TRANSFER FOR HIGH-ENERGY--ETC(U)
OCT 80 M O SCULLY AFOSR-79-0122

UNCLASSIFIED

AFOSR-TR-81-0108

NL

1 of 1
AD
A095 706

END
DATE
FILMED
3 81
DTIC

19
AFOSR/TR-81-0108

13

LEVEL II

AD A 095706

STUDY OF CHEMICAL REACTIONS AND ENERGY TRANSFER
FOR HIGH-ENERGY AND HIGH-POWER LASERS.

9 Final Technical Report 1 Jul 7-11-1980

by

15 Professor Marlan O. Scully, Principal Investigator

October 1980

DTIC
ELECTE
MAR 0 2 1981

E

11
Prepared for the
Air Force Office of Scientific Research (AFSC)
Bolling AFB, DC 20332
Under grant AFOSR-79-0122

Approved for public release;
distribution unlimited.

Optical Sciences Center
University of Arizona
Tucson, Arizona 85721

DEC FILE COPY

81 2 27 074

Unclassified

SECURITY CLASSIFICATION OF THIS PAGE (When Data Entered)

REPORT DOCUMENTATION PAGE		READ INSTRUCTIONS BEFORE COMPLETING FORM
1. REPORT NUMBER AFOSR-TR- 81 - 0108 ✓	2. GOVT ACCESSION NO. AD-A095706	3. RECIPIENT'S CATALOG NUMBER
4. TITLE (and Subtitle) Study of Chemical Reactions and Energy Transfer for High-Energy and High-Power Lasers		5. TYPE OF REPORT & PERIOD COVERED Final Report 7/1/79 - 8/31/80
7. AUTHOR(s) Marlan O. Scully		6. PERFORMING ORG. REPORT NUMBER
9. PERFORMING ORGANIZATION NAME AND ADDRESS Optical Sciences Center University of Arizona Tucson, AZ 85721		8. CONTRACT OR GRANT NUMBER(s) AFOSR-79-0122 ✓
11. CONTROLLING OFFICE NAME AND ADDRESS Air Force Office of Scientific Research (AFSC)/NP Bolling AFB, DC 20332		10. PROGRAM ELEMENT, PROJECT, TASK AREA & WORK UNIT NUMBERS 61102F 2301/A1
14. MONITORING AGENCY NAME & ADDRESS (if different from Controlling Office)		12. REPORT DATE 31 October 1980
		13. NUMBER OF PAGES 33
		15. SECURITY CLASS. (of this report) Unclassified
		15a. DECLASSIFICATION/DOWNGRADING SCHEDULE
16. DISTRIBUTION STATEMENT (of this Report) Approved for Public Release, Distribution Unlimited		
17. DISTRIBUTION STATEMENT (of the abstract entered in Block 20, if different from Report)		
18. SUPPLEMENTARY NOTES		
19. KEY WORDS (Continue on reverse side if necessary and identify by block number) Chemical Laser Molecular Collisions Energy Transfer Chemiluminescence		
20. ABSTRACT (Continue on reverse side if necessary and identify by block number) The purpose of this project was to perform theoretical and experimental investigation on reactive and nonreactive collision processes that occur in chemical laser systems. The theoretical investigation was focused on developing reliable and tractable numerical techniques that describe the dynamics of the collision processes. The experimental effort was devoted to a chemical laser scheme based on gas phase chemiluminescence reactions that allows pre-mixing of the reagents.		

DD FORM 1 JAN 73 1473

Unclassified

SECURITY CLASSIFICATION OF THIS PAGE (When Data Entered)

TABLE OF CONTENTS

I. ABSTRACT	1
II. SCIENTIFIC BACKGROUND	1
III. OVERVIEW OF THE WORK PERFORMED	4
A. A New Approach to Molecular Collisions: Statistical Quasi-Classical Method	5
B. Modification of the Semiclassical Method: Trajectory- Based Decoupling Scheme	7
C. Laser Initiated Chemiluminescence Experiments	9
IV. PUBLICATIONS	10
APPENDIX A. A New Approach to Molecular Collisions: Statistical Quasiclassical Method	11
APPENDIX B. A New Semiclassical Decoupling Scheme for Electronic Transitions in Molecular Collisions: Application to Vibrational-to-Electronic Energy Transfer	16
APPENDIX C. Pulsed Visible Chemiluminescence Experiments	23

Accession For	
NTIS GRA&I	<input checked="" type="checkbox"/>
DTIC TAB	<input type="checkbox"/>
Unannounced	<input type="checkbox"/>
Justification	
By	
Distribution/	
Availability Codes	
Avail and/or	Special
Dist	
A	

AIR FORCE OFFICE OF SCIENTIFIC RESEARCH (AFSC)
 NOTICE OF SUBMITTAL TO THE
 This technical report is being submitted to the AFSC and is
 approved for distribution under the AFSC-12 (7b).
 Distribution is unlimited.
 A. D. BLOOM
 Technical Information Officer

I. ABSTRACT

The purpose of this project was to perform theoretical and experimental investigation on reactive and nonreactive collision processes that occur in chemical laser systems. The theoretical investigation was focused on developing reliable and tractable numerical techniques that describe the dynamics of the collision processes. The experimental effort was devoted to a chemical laser scheme based on gas phase chemiluminescence reactions, which allows premixing of the reagents.

II. SCIENTIFIC BACKGROUND

Chemical lasers (for example, HF, DF, and iodine) have efficiently achieved power outputs of hundreds of kilowatts. So far, our understanding of these lasers is hampered by our inability to predict and interpret the energy distribution in the collision processes that pump the lasing states. The difficulty is not so much in understanding the physical laws that govern these processes as in solving the equations that exactly describe them; the equations are much too complicated to be solvable. Therefore, researchers working with chemical laser systems would like to see the development of a technique to solve the equations that is both accurate and numerically tractable. Since the exact quantum-mechanical approach is not numerically tractable in general, one must rely on various approximate results. The most popular approximate technique for describing molecular collisions is the classical trajectory method, in which the dynamics of collisions are described completely by

classical mechanics rather than quantum mechanics. When this technique is combined with the commonly used procedure for classifying trajectories as to their initial and final states, it is often referred to as the quasi-classical (QC) method. Although the QC method is easy to apply and interpret, it is often not sufficiently accurate in describing microscopic state-to-state aspects of collisions which are important in the study of chemical laser systems. Furthermore, because the method is intrinsically classical, it is not capable of describing classically forbidden processes resulting from quantum tunneling. To overcome this weakness of the QC method, a method usually called a semiclassical (SC) method was introduced. In this method, classical trajectories are allowed to take on complex values, thus enabling one to approximately describe classically forbidden processes. However, one here carries the burden of working with complex-valued trajectories, which are very difficult to handle. It therefore seems highly desirable to develop a new technique that combines to a maximum degree the simplicity of the QC method with the accuracy of the fully quantum-mechanical (QM) method. This is where our theoretical effort under Grant No. AFOSR-79-0122 has been directed.

Chemical lasers such as HF, HCl, and CO operate on vibrational or rotational transitions and are thus infrared. A recent active field of research has been the development of visible wavelength chemical lasers that operate on electronic transitions. To achieve lasing on an electronic transition in a typical diatomic molecule, it is necessary to rapidly generate a supply of molecules in the upper

level of the laser transition. At visible wavelengths this requirement is difficult to satisfy with a traditional mixing-type chemical laser that employs chemical reactions which initiate spontaneously upon mixing of the reagents. An alternative scheme that we have pursued involves gas-phase chemiluminescence reactions that do not initiate until "triggered" by a suitable low-power ignition mechanism. Thus, reagents can be premixed, and a small input of optical or electrical energy can be used to produce an initial chain carrier species. The resulting chemical reaction is thus self-sustaining via branched chain reaction kinetics. Our experimental effort was devoted to this scheme, utilizing chemiluminescence reactions that are triggered by a pulsed laser.

III. OVERVIEW OF THE WORK PERFORMED

In research supported by Grant AFOSR-79-0122, we have accomplished the following:

1. Developed a new approach to molecular collisions that appears to have overcome several difficulties of the QC and SC methods.
2. Modified the SC method so as to accurately describe near-resonance vibrational-to-electronic energy transfer processes.
3. Obtained intense blue-green chemiluminescence from the $d^3\pi \rightarrow a^3\pi$ transition of C_2 by premixing ClO_2 with acetylene (C_2H_2) and triggering the reaction with an XeF excimer laser.

Progress in the above three areas is described in the following subsections. Further details can be found in the appended reports.

A. A New Approach to Molecular Collisions: Statistical Quasi-Classical Method

Our theoretical effort was focused on developing a technique that combines to a maximum degree the simplicity of the QC method and the accuracy of the QM method. This of course is the spirit with which the SC method was developed. To avoid complications due to the handling of complex-valued trajectories, we elected to keep the trajectories real, thus describing the dynamics of collisions completely by classical mechanics. However, we used a quantum statistical representation of initial and final states instead of the usual representation based on the classical probability distribution that is used in the QC method. Thus, our new method may be considered to be the classical trajectory method with a touch of quantum statistics in representing initial and final states. For this reason, we call our method the statistical quasi-classical (SQC) method.

The quantum statistical representation of the states seems to be most conveniently achieved by using the Wigner distribution function,

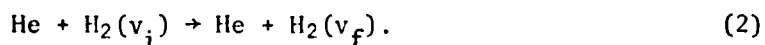
$$W(q,p,t) = \frac{1}{\pi\hbar} \int dx \exp(-2ipx/\hbar) \psi^*(q-x,t) \psi(q+x,t). \quad (1)$$

Roughly speaking, the Wigner function gives the quantum-mechanical probability distribution at time t in phase space (q,p) for the system described by the wavefunction $\psi(q,t)$. To use it in our SQC method, we first need to find the initial Wigner function $W(q,p,t = -\infty)$ corresponding to the initial state $\psi(q,t = -\infty)$. Each element (q,p) of the initial Wigner function is then propagated in time using the classical Hamilton equations of motion. This

propagation is achieved in practice by representing the initial Wigner distribution by a finite number, N , of points on an appropriate two-dimensional grid in the (q,p) plane and then integrating the Hamilton equations of motion for each of the N points (q,p) on the grid. The collection of the final values of q and p obtained after the integration constitutes the final Wigner distribution function $W(q,p,t = \infty)$, from which the transition probability can be obtained.

Since the SQC method contains some quantum-mechanical features not contained in the QC method, one might expect it to be able to at least partially describe classically forbidden processes. The chief disadvantage of the SQC method, on the other hand, is that it requires a large number of trajectories to be computed, as each element (q,p) of the Wigner distribution must be propagated. However, this is only a small disadvantage, considering the advantage of not having to deal with complex-valued trajectories.

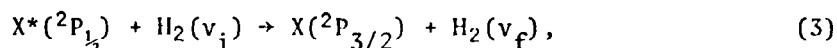
The SQC method was applied to the collinear inelastic collision,



Calculations clearly showed that the SQC method is more accurate than the QC method. They also indicated that the SQC method is, or at least has a potential to be, capable of accurately describing classically forbidden processes. It appears, therefore, that the SQC method represents an appealing alternative to the existing techniques for describing molecular collisions, especially when more accurate information is desired than can be obtained by the QC method and when the fully QM method or the SC method is too difficult to handle.

B. Modification of the Semiclassical Method: Trajectory-Based Decoupling Scheme

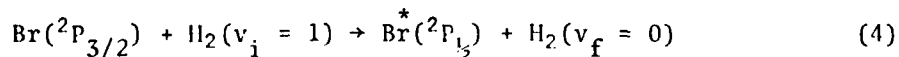
The major difficulty of the SC method in describing collision processes lies in the complexity of integrating complex-valued trajectories. One of the approximate schemes designed to alleviate this difficulty is the "decoupling" scheme, in which trajectories are assumed to take on real values except when they hit (avoided) crossing points at which electronic transitions may occur in the SC theory. The scheme then assumes that all but one appropriately chosen coordinate η and momentum P_η can be "frozen" at the crossing points and calculates the transition probability in a Stuckelberg manner, allowing only the "decoupled" coordinate η and momentum P_η to take on complex values. It is important to make an intelligent choice of the decoupled coordinate η if the approximation is to be reliable. The usual way of choosing it is to look at the structure of the potential energy surface in the neighborhood of crossing points and determine which component of momentum is most effective in leading to electronic transitions. For example, for the colinear collision



where X is either F or Br , the decoupled coordinate η was chosen to be the translational coordinate R . Although SC calculations with this choice of η yielded energy transfer probabilities in good agreement with the corresponding QM calculations for $X = F$, a strong disagreement was found for $X = Br$. This was attributed to the inability of the SC method to describe near-resonance processes involving

vibrational or rotational energy levels, because internal (vibrational and rotational) degrees of freedom are treated classically in the SC method. However, it is not entirely clear that resonance effects should be absent simply because internal motions are treated classically. A good agreement might be obtained with a better choice of the decoupled coordinate, even if we use the SC method or even the QC method. This is an important consideration because it determines whether one can use a numerically tractable technique (the QC method) to describe near-resonance processes of importance in chemical laser systems.

A better choice of the decoupled coordinate η , we believe, can be achieved by taking η to be the coordinate along the direction of motion at a crossing point. The reason for this particular choice can be found in the reprint of Appendix B (Lee, Lam, DeVries, and George). Here we only note that η determined by the above choice is generally different for different trajectories, and therefore has to be defined for each trajectory at each encounter with a crossing point. For this reason, the new decoupling scheme is called the trajectory-based decoupling scheme. QC calculations have been carried out for the near-resonance vibrational-to-electronic energy transfer process



using the trajectory-based decoupling scheme. The agreement with the QM calculations is much better with the trajectory-based scheme than with the old scheme. Furthermore, as we artificially varied the spin-orbit splitting of Br around the fixed vibrational frequency of H_2 ,

the new scheme clearly reproduced the resonance peak structure of the transition probability, whereas the old scheme failed. It therefore seems that our new scheme opens the door for the QC method to describe near-resonance energy transfer processes.

The work described in this section was carried out in cooperation with Prof. Thomas F. George and his coworkers at the University of Rochester.

C. Laser-Initiated Chemiluminescence Experiments

To obtain chemiluminescence from C_2 using the premixing technique, we first generated chlorine dioxide (ClO_2) by passing Cl_2 gas over $NaClO_2$ crystals. The ClO_2 was then collected into the reaction cell, to which acetylene (C_2H_2) was added to allow it to be mixed with the ClO_2 . A single 10-mJ, 20-nsec pulse of 3500 Å light from a XeF excimer laser was then used to detonate the mixture. The detonation resulted in an intense blue-green chemiluminescence, which was easily identified as the $C_2(d^3\pi \rightarrow a^3\pi)$ Swan bands. From the observation of the temporal behavior of the chemiluminescence, we found that the rise time of the pulse is typically 30 to 50 μ sec, while the "burn-time" exceeds 1 msec. The time delay before the rapid onset of light emission was on the order of the time required for a shock front to travel from the laser input window to the side-arm where light emission was observed. We do not know the exact mechanism of reaction and therefore cannot speculate in detail regarding the kinetics of the reaction. The blue-green chemiluminescence from the C_2 Swan band was also observed from

$\text{HN}_3 + \text{C}_2\text{H}_2 + \text{N}_2\text{O} + \text{He}$ mixtures using a single 20-mJ, 20-nsec pulse of 2490-Å KrF excimer laser light. In addition, strong CN violet band emission was also observed from this mixture. To determine whether a chemically pumped C_2 laser is possible from the schemes described above, however, further investigation is necessary on the kinetics of the reactions involved.

The work described in this section was carried out in cooperation with Dr. David Benard at AFWL.

IV. PUBLICATIONS

The following publications, produced in conjunction with this work, are reproduced as appendixes to this report:

Hai-Woong Lee and Marlan O. Scully, "A new approach to molecular collisions: Statistical quasiclassical method," J. Chem. Phys. 73(5): 2238-2242, 1 Sept. 1980.

Hai-Woong Lee, Kai S. Lam, Paul L. DeVries, and Thomas F. George, "A new semiclassical decoupling scheme for electronic transitions in molecular collisions: Application to vibrational-to-electronic energy transfer," J. Chem. Phys. 73(1): 206-212, 1 July 1980.

M. D. Burrows and D. J. Benard, "Pulsed visible chemiluminescence experiments," Laser Digest, summer 1980.

A new approach to molecular collisions: Statistical quasiclassical method^{a)}

Hai-Woong Lee and Marlan O. Scully

*Department of Physics and Optical Sciences Center, University of Arizona, Tucson, Arizona 85721
and Projektgruppe für Laserforschung der Max-Planck Gesellschaft, D-8046 Garching bei München,
West Germany*

(Received 25 March 1980; accepted 12 May 1980)

A new approach is presented in which classical mechanics is combined with quantum statistics to describe molecular collisions. In this approach, the dynamics of collisions is described by classical trajectories as in the widely used quasiclassical method. However, initial and final internal states are represented in phase space in a quantum statistical way, using the Wigner distribution function. Results of calculations performed on a collinear He-H₂ collision indicate that this new method is more accurate than the quasiclassical method, especially when the initial vibrational energy is low. Moreover, the new method is capable of describing classically forbidden processes that cannot be accounted for by the quasiclassical method.

I. INTRODUCTION

The classical trajectory method is probably the most popular technique for describing the dynamics of molecular collisions.^{1,2} As the name of the method implies, the colliding molecules obey Hamilton's equations of motion. The technique is often referred to as the quasiclassical (QC) method when combined with the commonly used procedure for classifying trajectories as to their initial and final states. The strength of the QC method is that it is easy to apply and requires less computer time and expense than the accurate quantum-mechanical (QM) method. However, the QC method is often not sufficiently accurate in describing microscopic state-to-state aspects of collisions. Furthermore, the QC method, due to its intrinsically classical nature, is not capable of describing classically forbidden processes resulting from quantum mechanical tunneling. Therefore, it is highly desirable to develop a technique that overcomes the weakness of the QC method, while retaining its strong points as much as possible. Progress has been made along this direction in recent years.³⁻⁵

In this paper, we introduce an approach termed the statistical quasiclassical (SQC) method, which is essentially the classical trajectory method combined with a quantum statistical representation of initial and final states. The idea of the method stems from the fact that the usual assignment of initial conditions in the QC method is often inaccurate from the quantum mechanical point of view. For example, the selection of the vibrational phase of a harmonic oscillator is based on the probability distribution resulting from the classical harmonic motion. This, however, approaches the correct quantum mechanical distribution only in the limit of high vibrational energy. One might expect to obtain higher accuracy by using an initial assignment based on the quantum mechanical nature of the system being investigated. This consideration immediately leads to the idea of using an appropriate probability distribution function in phase-space, derived using quantum mechanical wave functions. We choose for this purpose the Wigner dis-

tribution function,^{6,7} which has been widely used in the past for describing a variety of systems.⁸⁻¹² Thus, in our SQC method, initial internal states are represented by the corresponding Wigner distribution, which then is propagated in time using the classical trajectory method. The resulting final Wigner distribution carries information on the final state, and therefore can be used to obtain transition probabilities. The Wigner distribution function yields the correct quantum mechanical probability distribution for both position and momentum of the system under consideration. Therefore, the SQC method contains at least some quantum mechanical features not contained in the QC method. In this regard, it is of primary interest to see how well the SQC method can describe classically forbidden processes. In Sec. II we give a brief review of the basic properties of the Wigner distribution function, useful for the development of the SQC method. Section III follows with a description of the SQC method, and its application to a collinear He-H₂ collision is described in Sec. IV.

II. THE WIGNER DISTRIBUTION FUNCTION

The Wigner distribution function $W(q, p, t)$ may be defined as the Fourier inverse of the characteristic function

$$C(\xi, \eta, t) = \int dq \psi^*(q, t) \exp[i(\xi \hat{q} + \eta \hat{p})] \psi(q, t) \\ = \text{Tr} \{ \rho(\hat{q}, \hat{p}, t) \exp[i(\xi \hat{q} + \eta \hat{p})] \}, \quad (1)$$

i. e.,

$$W(q, p, t) = \frac{1}{4\pi^2} \int d\xi \int d\eta \exp[-i(\xi q + \eta p)] \\ \times \left(\int dq \psi^*(q, t) \exp[i(\xi \hat{q} + \eta \hat{p})] \psi(q, t) \right) \\ = \text{Tr} [\rho(\hat{q}, \hat{p}, t) \delta(q - \hat{q}) \delta(p - \hat{p})]. \quad (2)$$

Here ξ and η are real parameters, \hat{q} and \hat{p} denote coordinate and momentum operators, and q and p corresponding eigenvalues. It can be easily shown⁷ that Eq. (2) reduces to

$$W(q, p, t) = \frac{1}{\pi \hbar} \int dx \exp\left(\frac{-2ipx}{\hbar}\right) \psi^*(q - x, t) \psi(q + x, t), \quad (3)$$

^{a)} Research sponsored by the Air Force Office of Scientific Research under Grant No. AFOSR-79-0122.

an expression first given by Wigner.⁶ If we expand ψ in terms of an orthonormal set of eigenfunctions

$$\psi(q, t) = \sum_n a_n(t) \psi_n(q), \quad (4)$$

Eq. (3) becomes

$$W(q, p, t) = \sum_n \sum_m a_n^*(t) a_m(t) \omega_{nm}(q, p), \quad (5)$$

where

$$\omega_{nm}(q, p) = \frac{1}{\pi \hbar} \int dx \exp\left(\frac{-2ipx}{\hbar}\right) \psi_n^*(q-x) \psi_m(q+x). \quad (6)$$

It can also be shown⁷ that the functions ω_{nm} 's form a complete orthogonal set in the phase space (q, p) ,

$$\int dq \int dp \omega_{nm}^*(q, p) \omega_{n'm'}(q, p) = \frac{\delta_{nn'} \delta_{mm'}}{2\pi \hbar}, \quad (7a)$$

$$\sum_n \sum_m \omega_{nm}(q, p) \omega_{nm}^*(q', p') = \frac{\delta(q-q') \delta(p-p')}{2\pi \hbar}. \quad (7b)$$

If we integrate the function W given by Eq. (3) over p , we obtain

$$\int dp W(q, p, t) = \psi^*(q, t) \psi(q, t). \quad (8a)$$

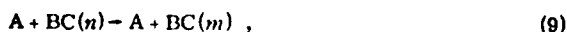
Similarly, we get

$$\int dq W(q, p, t) = \tilde{\psi}^*(p, t) \tilde{\psi}(p, t), \quad (8b)$$

where $\tilde{\psi}(p, t)$ is the Fourier inverse of $\psi(q, t)$, or the wave function in the momentum space. Equation (8) indicates that the Wigner distribution function yields the correct quantum mechanical probability distribution in both coordinate and momentum spaces.

III. STATISTICAL QUASICLASSICAL METHOD

In this section, we describe our new approach, the SQC method. In principle, this method can be applied to any type of collision process. For convenience of presentation, however, we consider a nonreactive atom-diatom collision



where n and m refer to any relevant set of initial and final quantum numbers. We denote the translational coordinates and momenta collectively by Q and P and the internal coordinates and momenta by q and p . At the initial time $t = -\infty$, the diatom BC is prepared in its n th eigenstate

$$\psi_{BC}(q, t = -\infty) = \psi_n(q). \quad (10)$$

In our approach, this initial state is represented by the corresponding Wigner distribution function, which can be written by using Eqs. (5) and (6) as

$$W(q, p, t = -\infty) = \omega_{nn}(q, p) = \frac{1}{\pi \hbar} \int dx \exp\left(\frac{-2ipx}{\hbar}\right) \times \psi_n^*(q-x) \psi_n(q+x). \quad (11)$$

The initial translational coordinates and momenta are specified as usual: the initial Q corresponds to an arbitrarily large separation of A and BC at which the A-BC

interaction is negligible, and the initial P is determined by the collision energy. Now, our system, $A + BC$, initially specified by Q, P and $W(q, p, t = -\infty)$, evolves in time according to Hamilton's equations of motion. To integrate Hamilton's equations, we first represent the initial distribution $W(q, p, t = -\infty)$ by a finite number (N) of points on an appropriate two-dimensional grid in the (q, p) plane. The integration is then carried out N times for fixed initial values Q, P and for each point (q, p) on the grid. The collection of final values of q and p obtained after the integration constitutes the final distribution function

$$W(q, p, t = \infty) = \sum_i \sum_j a_i^*(t = \infty) a_j(t = \infty) \omega_{ij}(q, p), \quad (12)$$

corresponding to the final state of the diatom BC,

$$\psi_{BC}(q, t = \infty) = \sum_i a_i(t = \infty) \psi_i(q). \quad (13)$$

The transition probability $n \rightarrow m$ can then be obtained from

$$P_{m \leftarrow n} = |a_m(t = \infty)|^2 = 2\pi \hbar \int dq \int dp \omega_{nm}(q, p) W(q, p, t = \infty), \quad (14)$$

where the orthogonality relation, Eq. (7a), has been used in obtaining Eq. (14). Thus, the recipe to obtain the transition probability $P_{m \leftarrow n}$ using the present SQC method is simple: one first finds the initial Wigner distribution ω_{nn} from Eq. (11) and then obtains the final Wigner distribution $W(q, p, t = \infty)$ by integrating Hamilton's equations of motion for each element (q, p) of ω_{nn} . The transition probability can then be obtained by Eq. (14).

It should be noted that the statistical representation of the initial state according to Eq. (11) is what differentiates the SQC method from the usual QC method. The uncertainty relation required by quantum mechanical considerations is contained in this statistical representation, and for this reason the SQC method is expected to be able to describe classically forbidden processes. It should also be noted that in our method the Wigner distribution function is used only to represent the initial and final states, and the collision dynamics occurring between the initial and final times is still governed completely by classical mechanics. This differs from other works utilizing the Wigner distribution function,⁸⁻¹² in which the dynamics is governed by the Schrödinger equation of motion. One difficulty in using the essentially quantum mechanical Wigner distribution function to determine initial and final conditions for purely classical equations of motion is that some quantum mechanical features of the Wigner distribution function are lost during the classical dynamical evolution. This is a fundamental limitation on the SQC method in its present form. This point will be further illustrated in the next section. In spite of this difficulty, our desire to keep the calculational procedure at an elementary level provides strong incentive for working with the classical equations of motion.

IV. EXAMPLE

To illustrate our approach, we model the collinear He-H₂ collision as follows: H₂ is approximated by a

harmonic oscillator, and the He-H₂ interaction is an exponential repulsion between He and the closer end of H₂. This system has been extensively studied in the past, quantum mechanically^{13,14} as well as semiclassically.¹⁵⁻¹⁸ We choose the potential parameters according to Secrest and Johnson,¹³ and one should consult their paper for details of the system. Here we only need to discuss those features that are newly encountered in our approach.

Let us assume that the harmonic oscillator (H₂) is initially in its n th eigenstate

$$\psi_n(q) = N_n H_n(\alpha q) \exp(-\frac{1}{2} \alpha^2 q^2), \quad (15)$$

where $\alpha = (\mu \omega_0 / \hbar)^{1/2}$; μ and ω_0 are, respectively, the mass and the angular frequency of the harmonic oscillator; N_n is the normalization constant; and H_n denotes the n th Hermite polynomial. Then the initial Wigner distribution function is given by Eqs. (5) and (6) as

$$W(q, p, -\infty) = \omega_{nn}(q, p) = \frac{N_n^2}{\pi \hbar} \int dx \exp\left(\frac{-2ipx}{\hbar}\right) H_n(\alpha q - \alpha x) \times \exp\left[-\frac{1}{2} \alpha^2 (q - x)^2\right] H_n(\alpha q + \alpha x) \exp\left[-\frac{1}{2} \alpha^2 (q + x)^2\right]. \quad (16)$$

By straightforward algebra, we obtain

$$\omega_{nn}(q, p) = \frac{(-1)^n}{\pi \hbar} \exp\left[-\left(\alpha^2 q^2 + \frac{p^2}{\alpha^2 \hbar^2}\right)\right] L_n\left(2\alpha^2 q^2 + \frac{2p^2}{\alpha^2 \hbar^2}\right) \quad (17)$$

or

$$\omega_{nn}(q, p) = \omega_{nn}(y) = [(-1)^n / \pi \hbar] \exp(-y) L_n(2y), \quad (18)$$

where the energy parameter y is defined as

$$y = \alpha^2 q^2 + p^2 / \alpha^2 \hbar^2 = (2/\hbar \omega_0) (\frac{1}{2} \mu \omega_0^2 q^2 + p^2 / 2\mu), \quad (19)$$

and L_n refers to the n th Laguerre polynomial. For example,

$$\omega_{00}(y) = (1/\pi \hbar) \exp(-y), \quad (20a)$$

$$\omega_{11}(y) = (-1/\pi \hbar) (1 - 2y) \exp(-y). \quad (20b)$$

We note that the initial distribution depends only on the energy parameter y . This, however, is due to the assumption that the system is initially in an energy eigenstate. If the system is not in an energy eigenstate, the Wigner distribution function would contain off-diagonal elements ω_{ij} , $i \neq j$, which in general depend on q and p separately.

In order to numerically represent the initial distribution given by Eq. (17), we construct a two-dimensional rectangular grid in the (q, p) plane. The size and the density of the grid should be taken as the smallest ones with which the desired accuracy can be achieved. For our calculations of the He-H₂ collision, for example, 20×20 points in the rectangle connecting the four points $(\pm 2/\alpha, \pm 2\alpha \hbar)$ gives sufficiently accurate results for $n=1$. Each point (q_i, p_i) in the i th cell of the grid carries with it the weight

$$\omega_{nn}(q_i, p_i) = \omega_{nn}(y_i) = (-1)^n \exp(-y_i) L_n(2y_i) / \pi \hbar.$$

Starting with (q_i, p_i) and the initial values of the translational coordinates Q and momenta P , we now numerically

integrate Hamilton's equations of motion until the final condition is reached. As in the usual QC method, we then obtain the final energy of the oscillator or the corresponding final y value $y_i^{(f)}$.

The collection of these final y values, with the weight factor $\omega_{nn}(y_i)$ now associated with $y_i^{(f)}$, may be considered to represent the final Wigner distribution $W(y, t=\infty)$. The transition probability $n \rightarrow m$ can then be obtained by

$$\begin{aligned} P_{m \leftarrow n} &= 2\pi \hbar \int dq \int dp \omega_{nn}(q, p) W(q, p, t=\infty) \\ &\approx K' \int dy \omega_{nn}(y) W(y, t=\infty) \\ &\approx K \sum_i \omega_{nn}(y_i^{(f)}) \omega_{nn}(y_i), \end{aligned} \quad (21)$$

where K and K' are appropriate normalization constants.

We note here that the final Wigner distribution is considered to be a function of y , not of q and p separately. If we were to consider q and p as two independent variables, the physical distribution obtained would depend on the choice of the final time. However, since the final state is in general a superposition of energy eigenstates, the correct final Wigner distribution function should contain off-diagonal elements ω_{ij} , $i \neq j$, and therefore should depend on q and p separately. In other words, all information concerning the off-diagonal elements ω_{ij} , $i \neq j$, in the Wigner distribution is lost in our treatment. This is the price that we have to pay for using classical equations of motion to describe the dynamics. The same difficulty also exists in the initial Wigner distribution. One might argue that the initial distribution represented by the set of points on the grid is meaningless, in the sense that the distribution would be physically different for a different choice of the initial time. This difficulty, however, can be avoided at least numerically by taking sufficiently many points on the grid such that the difference is negligible. This is ensured in our calculations by increasing the number of points on the grid until the final results change little with a further increase.

Calculations have been carried out for transition probabilities of the He-H₂ system, using the proposed SQC method as well as the usual QC method. The results are shown in Table I and Fig. 1 for various initial translational and vibrational energies, along with the "exact" results of Secrest and Johnson.¹³ The SQC method is seen to yield reasonably accurate probabilities for the case $n=0$, i.e., when the oscillator is initially in its ground state. However, for $n=2$ the SQC method is almost as "inaccurate" as the QC method. It is not immediately clear why the SQC method becomes less accurate as n increases. The most interesting feature in our results is that the SQC method yields finite probabilities for the two classically forbidden processes; $0 \rightarrow 0$ for the case $E=20$ (in units of $\frac{1}{2} \hbar \omega_0$), and $1 \rightarrow 3$ for $E=12$ (see Table I). The same method, however, yields zero probability, within the accuracy of the method, for the other two classically forbidden processes; $2 \rightarrow 5$ for $E=16$ and $2 \rightarrow 4$ for $E=12$. This only means that the SQC method, as developed here, is capable of describing classically forbidden processes, but needs further

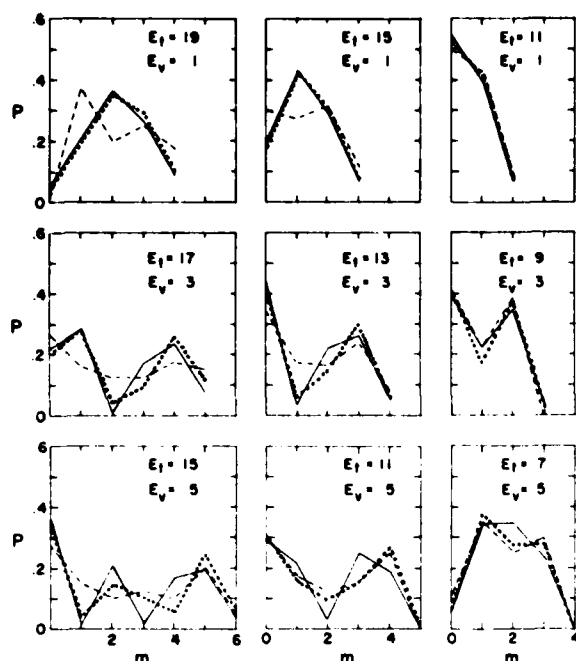


FIG. 1. Transition probabilities P as functions of final vibrational quantum numbers m , calculated from the quantum mechanical (solid lines) (Ref. 13), quasiclassical (dashed lines), and the statistical quasiclassical (dotted lines) methods. Initial translational and vibrational energies E_t and E_v are given in units of $\frac{1}{2}\hbar\omega_0$, where ω_0 is the vibrational frequency of H_2 .

improvement to be sufficiently accurate. In order to further study the accuracy of the SQC method in describing classically forbidden processes, we also made calculations for the case $E = 8$. In this case the initial energy is so low that most transitions are classically forbidden. The results of the SQC and QC calculations are shown in Table II, along with the QM results of Secrest and Johnson.¹³ One sees that the SQC method is very accurate in this case. This is made more evident in Table III. Here the results of SQC and QC calculations are shown for a collinear He-HBr collision with $E = 12$ (in units of $\frac{1}{2}\hbar\omega_0$, where ω_0 is now the vibrational frequency of HBr). Also shown are the corresponding QM data of Clark and Dickinson.¹⁴ In this case all transitions are classically forbidden, as can be seen from the QC data. Nevertheless, the SQC method gives quite accurate probabilities for all the forbidden processes listed in Table III. On the other hand, the SQC method cannot accurately describe processes that have probabilities less than $\sim 10^{-3}$. For example, the QM calculations¹⁴ show that the transition $0 \rightarrow 2$ (and $2 \rightarrow 0$) has the probability $\sim 10^{-4}$. This, however, is beyond the accuracy of the SQC method in its present form.

A useful criterion by which to judge the accuracy of a method is whether forward and reverse probabilities computed using that method are equal at the same total energy; i.e., whether the transition probabilities obey microscopic reversibility. QM probabilities obey this principle, whereas QC ones often badly violate it, as can be seen in Tables I and II. Tables I, II, and III also

TABLE I. Transition probabilities for a collinear He- H_2 collision calculated from the quantum mechanical (QM)^a (Ref. 13), quasiclassical (QC), and the proposed statistical quasiclassical (SQC) methods. The total initial energy E is measured in units of $\frac{1}{2}\hbar\omega_0$, where ω_0 is the vibrational frequency of H_2 .

	QM ^b	QC ^b	SQC ^b	QM ^c	QC ^c	SQC ^c	QM ^d	QC ^d	SQC ^d
0 \rightarrow 0	(0.060) ^e	0 ^e	0.046 ^e	(0.204)	0.300	0.187	(0.538)	0.500	0.520
1	0.218	0.375	0.202	0.434	0.275	0.422	0.394	0.425	0.412
2	0.366	0.200	0.351	0.291	0.313	0.314	0.068	0.075	0.068
3	0.267	0.250	0.294	0.071	0.113	0.077			
4	0.089	0.175	0.106						
1 \rightarrow 0	0.218	0.263	0.199	0.434	0.350	0.420	0.394	0.388	0.411
1	(0.286)	0.163	0.285	(0.034)	0.175	0.065	(0.244)	0.225	0.176
2	0.009	0.125	0.042	0.220	0.163	0.151	0.345	0.388	0.385
3	0.170	0.125	0.091	0.261	0.238	0.302	0.037 ^e	0 ^e	0.028 ^e
4	0.240	0.175	0.262	0.051	0.075	0.061			
5	0.077	0.150	0.121						
2 \rightarrow 0	0.366	0.275	0.346	0.291	0.300	0.309	0.068	0.100	0.065
1	0.009	0.150	0.038	0.220	0.175	0.163	0.345	0.350	0.374
2	(0.207)	0.100	0.143	(0.034)	0.125	0.101	(0.348)	0.250	0.280
3	0.018	0.125	0.109	0.250	0.150	0.157	0.233	0.300	0.281
4	0.169	0.100	0.052	0.189	0.250	0.270	0.006 ^e	0 ^e	0 ^e
5	0.191	0.200	0.245	0.016 ^e	0 ^e	0 ^e			
6	0.037	0.050	0.068						

^aQuantum mechanical probabilities for elastic transitions given in parentheses are upper bounds.

^b $E = 20$.

^c $E = 16$.

^d $E = 12$.

^eClassically forbidden processes.

TABLE II. Transition probabilities for a collinear He-H₂ collision calculated from the quantum mechanical (QM)^a (Ref. 13), quasiclassical (QC), and the statistical quasiclassical (SQC) methods.

	QM ^b	QC ^b	SQC ^b
0 → 0	(0.892)	0.738	0.893
1	0.108	0.263	0.107
1 → 0	0.108	0.238	0.106
1	(0.850)	0.648	0.863
2	0.042	0.075	0.031
2 → 1	0.042 ^c	0 ^c	0.033 ^c
2	(0.957)	1	0.967
3	0.001 ^c	0 ^c	0 ^c

^aQuantum mechanical probabilities for elastic transitions given in parentheses are upper bounds.

^bE = 5 in units of $\frac{1}{2}h\nu_0$, where ν_0 is the vibrational frequency of H₂.

^cClassically forbidden processes.

show that SQC probabilities do obey microscopic reversibility to a good approximation. This is one good indication that the SQC method is superior to the QC method.

We have shown that the SQC method yields more accurate probabilities than the QC method for collinear He-H₂ and He-HBr collisions. One should keep in mind, however, that the QC method fares unfavorably for the particular systems chosen for our calculations. Systems with low particle masses offer a stringent test of the QC method. Furthermore, quantum tunneling effects manifest themselves more strongly in a collinear collision than in a realistic three-dimensional collision. For systems in which quantum effects are small and the QC method fares well, the use of the SQC method may not be fully justified. This is particularly so because the SQC method requires a large number of trajectories—typically an order of magnitude more than required in the QC method—to be computed, as each element (q_i, p_i) of the Wigner distribution must be propagated. In fact, this additional computational effort represents a major disadvantage of the SQC method as compared with the QC method. However, the SQC method still requires much less computational effort than the QM method, especially when the collision energy is high and a large number of channels need to be considered. This is because the number of trajectories required to be computed in the SQC method does not increase rapidly with respect to the collision energy, whereas the QM method goes rapidly out of reach as the collision energy is increased. Perhaps the strongest point in favor of the

TABLE III. Transition probabilities for a collinear He-HBr collision calculated from the quantum mechanical (QM)^a (Ref. 14), quasiclassical (QC), and the statistical quasiclassical (SQC) methods.

	QM ^b	QC ^b	SQC ^b
0 → 0	(0.976)	1	0.975
1	0.024 ^c	0 ^c	0.025 ^c
1 → 0	0.024 ^c	0 ^c	0.025 ^c
1	(0.960)	1	0.956
2	0.016 ^c	0 ^c	0.019 ^c
2 → 1	0.016 ^c	0 ^c	0.019 ^c
2	(0.980)	1	0.978
3	0.005 ^c	0 ^c	0.003 ^c

^aQuantum mechanical probabilities for elastic transitions given in parentheses are upper bounds.

^bE = 12 in units of $\frac{1}{2}h\nu_0$, where ν_0 is the vibrational frequency of HBr.

^cClassically forbidden processes.

SQC method is that quantum tunneling effects are described with real classical trajectories. This represents an important improvement over the semiclassical collision theory³ in which one carries the burden of working with complex-valued trajectories.

- ¹D. L. Bunker, *Meth. Comp. Phys.*, **10**, 287 (1971).
- ²R. N. Porter and L. M. Raff, "Dynamics of Molecular Collisions," in *Modern Theoretical Chemistry*, edited by W. H. Miller (Plenum, New York, 1976), Part I.
- ³W. H. Miller, *Adv. Chem. Phys.*, **25**, 69 (1970).
- ⁴J. C.ully, in Ref. 2.
- ⁵H. W. Lee, K. S. Lam, P. L. DeVries, and L. F. George, *J. Chem. Phys.*, **73**, 206 (1980).
- ⁶E. Wigner, *Phys. Rev.*, **40**, 719 (1932).
- ⁷J. E. Moyal, *Proc. Cambridge Philos. Soc.*, **45**, 99 (1949).
- ⁸J. P. Gordon, *Phys. Rev.*, **161**, 367 (1967).
- ⁹M. Lax and H. Yuen, *Phys. Rev.*, **172**, 362 (1968).
- ¹⁰J. H. Marburger and W. H. Louisell, *Phys. Rev.*, **166**, 174 (1969).
- ¹¹J. C. Goldstein and M. O. Scully, *Phys. Rev.*, **167**, 1084 (1973).
- ¹²J. Heller, *J. Chem. Phys.*, **65**, 1289 (1976).
- ¹³D. Secrest and B. R. Johnson, *J. Chem. Phys.*, **45**, 456 (1966).
- ¹⁴A. P. Clark and A. S. Dickinson, *J. Phys. B*, **6**, 164 (1973).
- ¹⁵W. H. Miller, *J. Chem. Phys.*, **53**, 3578 (1970).
- ¹⁶W. H. Miller and L. F. George, *J. Chem. Phys.*, **56**, 5668 (1972).
- ¹⁷J. R. Stine and R. A. Marcus, *J. Chem. Phys.*, **59**, 1115 (1973).
- ¹⁸J. W. Duff and D. G. Truhlar, *Chem. Phys.*, **9**, 743 (1975).

A new semiclassical decoupling scheme for electronic transitions in molecular collisions: Application to vibrational-to-electronic energy transfer

Hai-Woong Lee

Optical Sciences Center, University of Arizona, Tucson, Arizona 85721^{a)}

Kai S. Lam, Paul L. DeVries, and Thomas F. George^{b)}

Department of Chemistry, University of Rochester, Rochester, New York 14627^{c)}

(Received 24 January 1980; accepted 25 March 1980)

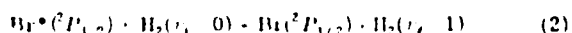
A new semiclassical decoupling scheme (the trajectory-based decoupling scheme) is introduced in a computational study of vibrational-to-electronic energy transfer for a simple model system that simulates collinear atom-diatom collisions. The probability of energy transfer (P) is calculated quasiclassically using the new scheme as well as quantum mechanically as a function of the atomic electronic-energy separation (λ), with overall good agreement between the two sets of results. Classical mechanics with the new decoupling scheme is found to be capable of predicting resonance behavior whereas an earlier decoupling scheme (the coordinate-based decoupling scheme) failed. Interference effects are not exhibited in P vs λ results.

I. INTRODUCTION

Vibrational-electronic energy transfer processes such as



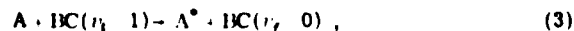
are of fundamental importance in the theory of molecular collision dynamics because they represent simple examples of electronically nonadiabatic collision processes.¹ An accurate description of Process (1), however, has not been without difficulties. The quantum mechanical (QM) coupled-channel approach, although most accurate and reliable of all existing methods, suffers from excessive computer time and expenses. Semiclassical (SC) and quasiclassical (QC) methods, as they have been further developed for the description of nonadiabatic processes,² are considered to give reliable results in many cases, although not as accurate as the QM method. However, as they treat internal molecular (vibrational and rotational) degrees of freedom classically, both methods are generally believed to be incapable of describing near-resonance processes involving vibrational or rotational energy levels. For example, SC calculations³ attempted on the near-resonance collinear collision process



yielded energy transfer probabilities in strong disagreement with the QM results.⁴ Thus, it seems that one has to rely only on fully QM calculations to correctly describe near-resonance processes. In view of this rather unfortunate situation, further development on the SC and QC methods seems desirable.

On the other hand, one might argue that it is not entirely clear that the resonance effects should be absent only because internal motions are treated classically. The disagreement between the QM and SC calculations on Process (2) may be due not to the failure inherent in the SC method but to the "decoupling" approximation⁵ made on the nonadiabatic coupling. In other words, one may only need to improve upon the approximation concerning the nonadiabatic coupling and still be able to use the SC or QC method for the description of near-resonance processes. This point deserves further investigation because the SC and in particular the QC method represent major computational simplifications over the QM method. Miller⁵ recently argued that, using an oversimplified model, the SC method (but not the QC method) should be able to correctly describe near-resonance collision processes. Unfortunately, no calculations have been carried out on realistic models or systems.

In this paper, we present a computational study of the resonance effects in the simplest of vibrational-to-electronic ($V \rightarrow E$) energy transfer processes: collinear atom-harmonic oscillator collision. Specifically, we are interested in the process



where the diatom BC is now approximated as a harmonic oscillator. The energy transfer probability P for Process (3) is calculated both quantum mechanically and quasiclassically as the electronic energy separation λ of the atom A is varied around a fixed value of the vibrational energy separation of the harmonic oscillator BC. The purpose of our study is to investigate the resonant process, and in particular, to propose (and test) a new decoupling scheme for the calculation of QC probabilities. This new scheme will be termed the trajectory-based decoupling scheme, for reasons to be discussed in Sec. IV. By investigating the QC probabilities thus calculated, it is hoped that we can approach an answer as to whether the QC (and SC) method may be used to study near-resonance processes.

^{a)}Research sponsored by the Air Force Office of Scientific Research under Grant No. AFOSR-79-0122.

^{b)}Alfred P. Sloan Research Fellow, 1976-80; Camille and Henry Dreyfus Teacher-Scholar, 1977-80.

^{c)}Research sponsored by the Air Force Office of Scientific Research under Contract No. F19620-78-C-0003, the National Aeronautics and Space Administration under Grant No. NSG-1195, and the National Science Foundation under Grant No. CHE77-27826.

In Sec. II the atom-harmonic oscillator model system is described. Section III follows with a description of the QM approach and results, and the QC counterpart is described in Sec. IV along with the newly proposed decoupling scheme. Results of this calculation and a comparison between this new decoupling scheme and the old one³ is presented in Sec. V.

II. THE MODEL

We consider the collinear energy transfer Process (3) between an atom A and a diatom BC approximated as a harmonic oscillator. For simplicity, the atom A is assumed to interact only with the nearer of B and C, and the interaction strength to be exponentially decreasing with respect to the internuclear distance. The potential surfaces are chosen to mimic those used for the Br-H₂ system in Ref. 4. The two adiabatic potential surfaces W_1 and W_2 are given by

$$W_1 = \{H_{11} + H_{22} - [(H_{22} - H_{11})^2 + 4H_{12}^2]^{1/2}\} / 2, \quad (4a)$$

$$W_2 = \{H_{11} + H_{22} + [(H_{22} - H_{11})^2 + 4H_{12}^2]^{1/2}\} / 2, \quad (4b)$$

where

$$H_{11} = A_1 \exp[-\alpha(R - \frac{1}{2}r - \rho_0)] + \frac{1}{2}m\omega_0^2(r - r_0)^2 + \frac{1}{2}\lambda, \quad (5a)$$

$$H_{22} = A_2 \exp[-\alpha(R - \frac{1}{2}r - \rho_0)] + \frac{1}{2}m\omega_0^2(r - r_0)^2 + \frac{7}{2}\lambda, \quad (5b)$$

and

$$H_{12} = \frac{\sqrt{2}}{3}\lambda. \quad (5c)$$

Here, R is the translational coordinate measured from the c.m. of BC to A, and r is the vibrational coordinate. The first terms in H_{11} and H_{22} represent the exponentially decreasing interaction strength between A and the nearer of B and C, and the second terms the harmonic oscillator potential function. The potential parameters, chosen to resemble those of the Br-H₂ system,⁴ are given as

$$A_1 = 3 \times 10^{-5}, \quad A_2 = 5 \times 10^{-5}, \quad \alpha = 3, \quad \rho_0 = 4,$$

$$\omega_0 = 0.02, \quad r_0 = 1.4, \quad m_A = 1.5 \times 10^5, \quad m_B = m_C = 2000,$$

where m_A, m_B, m_C are respectively masses of A, B, and C. Thus, the reduced mass m of the harmonic os-

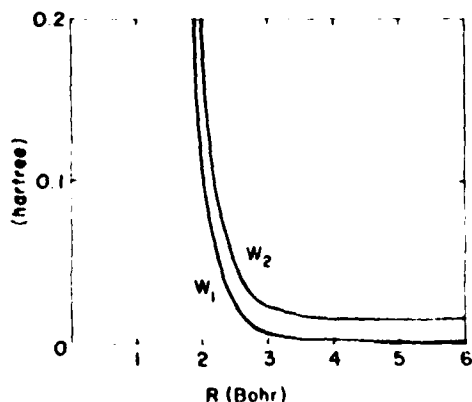


FIG. 1. The potential energy surfaces W_1 and W_2 vs the translational coordinate R . The vibrational coordinate is fixed at 1.4 and λ is assumed to be equal to 0.016.

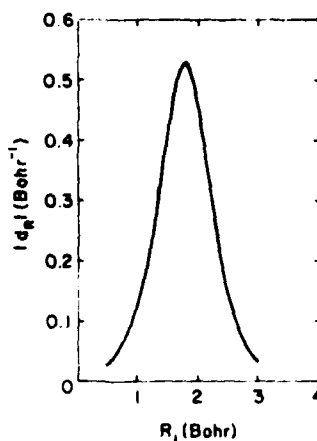


FIG. 2. The nonadiabatic coupling vs $R_1 = R - \frac{1}{2}r$. λ is assumed to be equal to 0.016.

cillator is given by 1000. All quantities throughout this paper are given in atomic units unless otherwise stated. For example, A_1 and A_2 are given in hartrees and ρ_0 and r_0 in bohrs. λ is the electronic energy separation of the two electronic levels of the atom A:

$$\lim_{R \rightarrow \infty} (W_2 - W_1) = \lambda.$$

One may assume that the two levels are separated by the spin-orbit interaction as in "Br." However, as noted in the Introduction, λ is considered to be a variable in our computational study and therefore is varied around the vibrational energy separation, $\hbar\omega_0 = 0.02$.

In Fig. 1, the potential energy surfaces W_1 and W_2 are drawn with respect to the translational coordinate R for a fixed vibrational coordinate, $r = r_0 = 1.4$, for the case $\lambda = 0.016$. It can be immediately seen that the potential difference $W_2 - W_1$ is a monotonically decreasing function of R , and therefore no avoided crossing occurs in our model system.

Having defined the potential energy surfaces, we now turn to the nonadiabatic coupling. The nonadiabatic coupling is given by the matrix elements⁶

$$d_R = \sum_m \sum_n \Gamma_{1m} \Gamma_{2n} \frac{\partial}{\partial R} H_{mn} / (W_2 - W_1), \quad (6a)$$

and

$$d_r = \sum_m \sum_n \Gamma_{1m} \Gamma_{2n} \frac{\partial}{\partial r} H_{mn} / (W_2 - W_1), \quad (6b)$$

where

$$\Gamma_{11} = \Gamma_{22} = H_{12} / [(W_1 - H_{11})^2 + H_{12}^2]^{1/2}, \quad (7a)$$

$$\Gamma_{12} = -\Gamma_{21} = H_{12} / [(W_2 - H_{11})^2 + H_{12}^2]^{1/2}. \quad (7b)$$

A straightforward calculation yields

$$d_R = -2d_r = -\frac{8\alpha}{9} \lambda^2 (Q - \frac{1}{2}\lambda) \left(Q^2 + \frac{8}{9} \lambda^2 \right)^{1/2} \left\{ Q - (Q^2 + \frac{8}{9} \lambda^2)^{1/2} \right\} \\ + \frac{8}{9} \lambda^2 \left\{ \left[Q + (Q^2 + \frac{8}{9} \lambda^2)^{1/2} \right]^2 + \frac{1}{9} \lambda^2 \right\}^{1/2}, \quad (8)$$

where

$$Q = (A_2 - A_1) \exp[-\alpha(R - \frac{1}{2}r - \rho_0)] + \frac{1}{2}\lambda. \quad (9)$$

It should be noted that d_R and d_r depend only on $R_1 = R - \frac{1}{2}r$, the separation between A and the nearer of B and C, not on R and r separately. In Fig. 2, $|d_R|$ is plotted

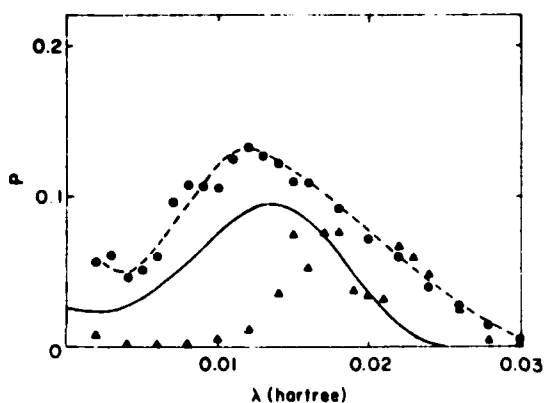


FIG. 3. The QM and QC probabilities vs λ for the $V-E$ energy transfer process (3). Collision energy = 0.055. The solid curve represents the QM probabilities and the circles represent the QC probabilities. The dotted curve is a smooth fit to the circles. The triangles represent the QC probabilities obtained using the decoupling scheme of Komornicki *et al.*

against R_1 for the case $\lambda = 0.016$. The nonadiabatic coupling is seen to be appreciable over the interval of about 2 bohr.

III. QUANTUM-MECHANICAL APPROACH

In this section, we report the results of QM calculations for the $V-E$ energy transfer process (3) performed on the model system described in the previous section. The solution to this problem was obtained in the usual manner by solving a set of close-coupled differential equations, subject to scattering boundary conditions. Since the interaction potentials are modeled as exponential functions, the required matrix elements over the harmonic oscillator basis can be performed analytically.⁷ The Light-Walker R -matrix method⁸ was employed to solve the close-coupled equations, and the step size and the initial and final limits of integration of the translational coordinate were varied until convergence of the

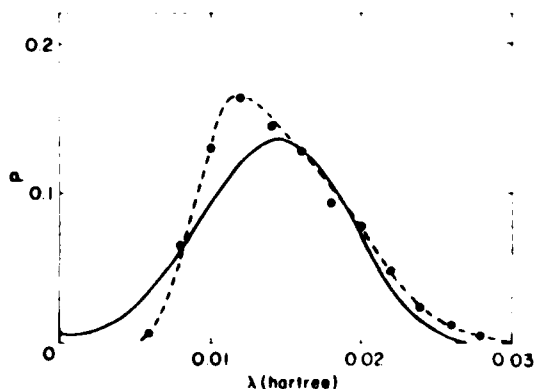


FIG. 4. The QM and QC probabilities vs λ for the $V-E$ energy transfer process (3). Collision energy = 0.045. The solid curve represents the QM probabilities and the circles represent the QC probabilities. The dotted curve is a smooth fit to the circles.

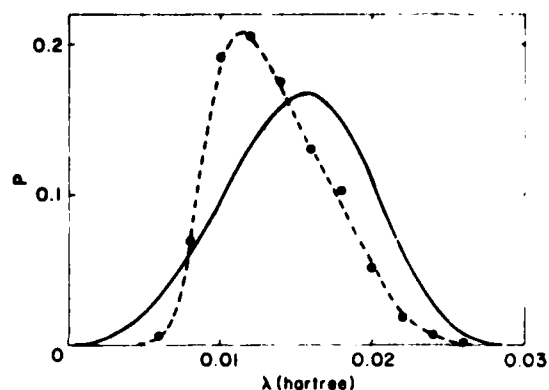


FIG. 5. The QM and QC probabilities vs λ for the $V-E$ energy transfer process (3). Collision energy = 0.035. The solid curve represents the QM probabilities and the circles represent the QC probabilities. The dotted curve is a smooth fit to the circles.

results was obtained. The results are shown in Figs. 3-5, in which the energy transfer probabilities are plotted with respect to λ for fixed collision energies. The following observations and interpretations can be made.

(1) Each curve has a single peak structure reflecting the $V-E$ resonance effect under consideration, and the resonance width tends to get smaller at lower collision energies. For the energy range considered here, the width is of the order of 0.01 hartree (≈ 0.27 eV).

(2) The peaks occur at values of λ smaller than the vibrational energy separation 0.02. In Table I, the peak positions along with the peak probabilities are listed. Of course, one would not expect the peaks to occur at exactly $\lambda = 0.02$ since the energy levels are perturbed by the collision. In fact, the curves are strongly asymmetric about $\lambda = 0.02$; the probabilities decrease rapidly as λ is increased from 0.02 while they go through a peak as λ is decreased from 0.02. This behavior can be understood if we note that the two potential surfaces representing the initial and the final quantum states do not cross if λ is greater than 0.02. On the other hand, if λ is smaller than 0.02, they do cross and the transition is more likely to be made. In particular, one might ex-

TABLE I. Peak positions and the probabilities at the peaks

Collision energy (hartree)	λ_{peak}	P
0.010	0.019	0.0919
0.015	0.018	0.130
0.020	0.017	0.151
0.025	0.017	0.169
0.030	0.016	0.172
0.035	0.016	0.166
0.040	0.015	0.154
0.045	0.015	0.135
0.050	0.014	0.115
0.055	0.013	0.0946

pect that the transition probability is the largest if the crossing occurs at a point of the maximum nonadiabatic coupling. A straightforward calculation shows that this condition is satisfied if $\lambda = 0.012$. According to Table I, the actual peaks occur at the values of λ between 0.012, a value derived from the above expectation, and 0.020, a value expected from the unperturbed energy level structure.

We have also calculated probabilities for the transition process

$$A + BC(r_i = 1) \rightarrow A^* + BC(r_f = 1) \quad (10)$$

using the same QM method. The branching ratio of the nonresonant process (10) to the near-resonant process (3) for a particular collision energy is shown in Table II for various values of λ .

IV. QUASICLASSICAL APPROACH-DECOUPLING SCHEME

In discussing nonadiabatic transitions in quasiclassical terms, one usually refers to the Landau-Zener type of approximations at (avoided) crossings of two surfaces. The two surfaces W_1 and W_2 of our model, however, do not possess an avoided crossing as seen in Sec. II. They nevertheless possess complex branch points at which the two surfaces cross provided that they are allowed to take on complex values and at which, in the SC theory, nonadiabatic transitions are allowed to take place. We therefore compute transition probabilities at the branch points using the method normally employed in the SC theory. However, the phase terms responsible for quantum interference effects are totally neglected and, for this reason, our approach is still termed quasiclassical² following the usual convention.

The branch points of our model system can be easily found by solving the equation

$$W_2(R_0, r_0) - W_1(R_0, r_0) = 0, \quad (11)$$

where R_0 and r_0 are now considered to assume complex values. Substituting Eqs. (4) and (5) into Eq. (11), we obtain

$$\{(A_2 - A_1) \exp[-\alpha(R_0 - \frac{1}{2}r_0 - \rho_0)] + \frac{1}{2}\lambda\}^2 + \frac{1}{4}\lambda^2 = 0, \quad (12)$$

which immediately yields the following equation for the branch points,

$$R_0 - \frac{1}{2}r_0 = u + iv, \quad (13a)$$

$$u - \rho_0 = \frac{1}{\alpha} \ln \frac{\lambda}{\lambda_2 - \lambda_1}, \quad (13b)$$

$$v = \frac{1}{\alpha} \cos^{-1} \frac{1}{2}. \quad (13c)$$

Even with this simple analytic structure of the branch points, a very large number of computational efforts are still needed to obtain transition probabilities, if the full complex valued trajectory method of the SC theory is to be used. A considerable computational simplification can be achieved, however, with the recently proposed decoupling scheme.³ Since we will use an improved version of this scheme in our calculations, a brief review of the scheme is in order.

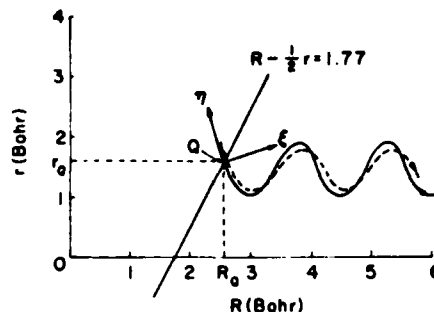


FIG. 6. Collision process viewed in the R - r plane. The branch points form a straight line. For the case $\lambda = 0.016$, the equation for the line is $R - \frac{1}{2}r = 1.77$. The solid and dotted curves represent a typical trajectory on the way in and out, respectively. The choice of the coordinates η and ξ according to the newly proposed decoupling scheme is illustrated at the point Q .

The decoupling scheme first invokes the localization of nonadiabatic transitions by assuming that the trajectories remain on the real axis except when they hit a point that coincides with the real part of the branch points. It then assumes that all but one appropriately chosen coordinate η and corresponding momentum P_η can be "frozen" at this point, and calculates the transition probability in a Stückelberg-like manner allowing only the "decoupled" coordinate η and momentum P_η to be analytically continued into the complex plane. The essence of the decoupling scheme is therefore to reduce a problem with multidegrees of freedom to one with a single degree of freedom analogous to an atom-atom collision.

We now wish to consider our atom-harmonic oscillator collision process within the decoupling picture. There are two degrees of freedom, translational and vibrational, in this collinear process as represented by the coordinates R and r (and corresponding momenta P_R and P_r). For this case, it is most convenient to use the R - r plane to discuss the motion of the system. In this plane, the real parts of the branch points given by Eq. (13b) forms a straight line, as shown in Fig. 6 for the case $\lambda = 0.016$. The system moves along one of the surfaces, W_1 or W_2 , according to Hamilton's equations of motion, until it encounters a point on the line. A typical trajectory is shown in Fig. 6, in which the line of the branch points is encountered twice during the collision process. Which points on the line the trajectory happens to hit, of course, depends on the initial conditions. To make our discussion definite, let us consider the point Q in Fig. 6 which can be represented by (R_0, r_0) in the R - r plane. To obtain the transition probability at this point using the decoupling scheme, we first need to choose a decoupled coordinate η and a frozen coordinate ξ , each of which can be in general a linear combination of R and r . In the scheme proposed by Komornicki *et al.*,³ η is chosen to be R and ξ to be r . The reason for the choice is that it is generally believed that the component of the momentum most effective in leading to nonadiabatic transitions is the one perpendicular to the line of the real parts of the branch points, and in their

TABLE II. The QM and QC branching ratios of Process (10) to Process (3).

λ	QM ^a	QC ^b	QC ^c
0.012	0.666	1.23	18.7
0.014	0.405	0.727	5.23
0.016	0.266	0.511	4.82
0.018	0.192	0.463	1.42
0.020	0.156	0.391	5.63
0.022	0.147	0.254	2.56

^aCollision energy = 0.055.^bCollision energy = 0.055. The new decoupling scheme is used.^cCollision energy = 0.055. The decoupling of Komornicki *et al.* is used.

study, this happens to be very nearly the translational momentum. Within this scheme the transition probability is given by

$$p = \exp(-2\delta), \quad (14)$$

where

$$\delta = \text{Im} \int_{R_Q}^{R_Q + i\epsilon} dR [k_1(R) - k_2(R)], \quad (15)$$

$$k_j(R) = \{2M[E - W_j(R, r_Q)]\}^{1/2}, \quad j = 1, 2, \quad (16)$$

$$M = m_A(m_B + m_C)/(m_A + m_B + m_C), \quad (17)$$

and E is the total energy. While the translational coordinate R and momentum P_R are allowed to proceed in the complex plane, the vibrational coordinate r and momentum P_r are assumed to be frozen at the values at Q ,

$$r = r_Q, \quad P_r = P_{r_Q}. \quad (18)$$

Thus, only the component of momentum in the R direction will be changed after the transition is made,

$$\frac{P_R^2}{2M} + W_j = \frac{P_R'^2}{2M} + W_{j'}, \quad (19)$$

where the prime is used to denote the quantities after the transition. The above choice of the decoupled and frozen coordinates, however, presents two immediate difficulties. First, the laws of classical mechanics are violated by assuming that both coordinate and momentum are frozen at finite nonzero values as dictated by Eq. (18). The position r can be fixed at r_Q only if P_{r_Q} is zero. Second, Eq. (19) suggests that the change in electronic energy represented by the potential jump $W_j - W_{j'}$ is accompanied by the change in translational energy rather than vibrational energy. This may incorrectly suppress $V-E$ energy transfer because the QM data in Table II show that $V-E$ energy transfer takes place more easily than translational-to-electronic ($T-E$) energy transfer in near-resonance processes. It now is not surprising that the $E-V$ energy transfer probabilities in the Br-HI system as calculated by Komornicki *et al.* were anomalously small. It also is evident that a more reasonable choice of the coordinates η and ξ will give a better result. We therefore propose the following in an attempt to overcome the above difficulties.

We choose η to be the coordinate along the direction

of motion and ξ perpendicular to it. This choice is illustrated in Fig. 6 at the point Q for the trajectory shown. Here, η and ξ take the form

$$\eta = R - \beta_Q r, \quad (20a)$$

$$\xi = R + r/\beta_Q, \quad (20b)$$

where

$$\beta_Q = -\dot{r}_Q/\dot{R}_Q, \quad (21)$$

and \dot{r}_Q and \dot{R}_Q are the vibrational and translational velocities, respectively, at Q . We note that η and ξ are in general different for different trajectories and therefore have to be defined for each trajectory at each encounter with a branch point. For this reason, our new decoupling scheme may be termed the trajectory-based decoupling scheme, as opposed to that of Komornicki *et al.*, which is based on the choice of an optimum coordinate. We will refer to the earlier scheme as the coordinate-based decoupling scheme.

The advantage of our choice of η and ξ is that $\dot{\xi}$ is always zero and therefore there is no conceptual difficulty in freezing this coordinate,

$$\xi = \xi_Q = R_Q + r_Q/\beta_Q, \quad P_\xi = 0. \quad (22)$$

The transition probability at Q is given by Eq. (14), where δ now becomes

$$\delta = \text{Im} \int_{\eta_Q}^{\eta_Q + i\epsilon} d\eta [k_1(\eta) - k_2(\eta)], \quad (23)$$

where

$$\eta_Q = R_Q - \beta_Q r_Q, \quad (24)$$

$$k_j(\eta) = \{2\mu_{\eta_Q}[E - W_j(\eta, \xi_Q)]\}^{1/2}, \quad j = 1, 2, \quad (25)$$

μ_{η_Q} , the reduced mass governing the motion of the system in the η direction, is shown in the Appendix to be given by

$$\mu_{\eta_Q} = \frac{M/\beta_Q^2 + m}{(\beta_Q + 1/\beta_Q)^2}, \quad (26)$$

and ν_{η_Q} is the imaginary part of the branch point that must satisfy Eqs. (13). Simple algebra immediately yields

$$\nu_{\eta_Q} = \frac{\beta_Q^2 + 1}{1 + \beta_Q/2} \nu. \quad (27)$$

Equations (20)–(27) now enable us to calculate for transition probabilities within the new decoupling scheme. Upon the completion of a transition, P_η is given a new value according to the energy conservation relation

$$\frac{P_\eta^2}{2\mu_{\eta_Q}} + W_j = \frac{P_\eta'^2}{2\mu_{\eta_Q}} + W_{j'}. \quad (28)$$

Because we are interested in the case of a low collision energy ($E_c \leq 0.055$), it occasionally happens during our QC calculations that there is not sufficient energy available for an upward transition. In this case, the formula introduced by Laing *et al.*⁶ is employed to calculate probabilities, with obvious modifications to account for the fact that now the decoupled coordinate η is the one to be integrated over. In the case of very high collision energies such that vibrational motion is

relatively weak, we expect the trajectory-based decoupling scheme to approach the coordinate-based one. Furthermore, in more general collision conditions not involving resonance transfer, the two decoupling schemes may also be equivalent.

V. RESULTS AND CONCLUSION

The method used for the QC calculations is the usual classical trajectory method^{10,11} modified to include the calculation of nonadiabatic transition probabilities with the trajectory-based decoupling scheme. The Hamilton equations of motion were numerically integrated using the fourth-order Adams-Moulton formulas with the fourth-order Runge-Kutta integration being employed to initiate the procedure. When the system encounters a branch point, the transition probability was computed as described in the previous section. The complex integration in Eq. (23) was carried out using the four-point Gauss-Legendre quadrature formula. Upon completion of the probability calculation, the integration of Hamilton equations was resumed. For a path starting on a new surface, the Runge-Kutta formula was again needed to initiate the integration with a new set of initial variables before the Adams-Moulton formula could be used. The system typically encountered two or four branch points during the collision process. For the case of four branch points, eight different paths must be considered. The final vibrational quantum number was assigned using the usual quasiclassical box. The total probability for the energy transfer process (3) was then obtained from the equation

$$P = \sum_i p_i / N, \quad (29)$$

where N is the total number of trajectories, p_i is the total transition probability for the i th trajectory that enters the box $v_f = 0$, and the summation runs over all such trajectories.

The results of the QC calculations are shown in Figs. 3, 4, and 5. The circles represent the QC probabilities actually obtained from the calculations, and the dotted curves are smooth fits to the circles.

In Fig. 3, the result of QC calculations using the coordinate-based decoupling scheme is also shown. The probabilities, represented by the triangles, are rather unstable with respect to the variation of λ , as can be seen from the apparent three-peak structure. Consequently, it is hard to judge whether this set of data contains any resonance effect in it. The superiority of the new decoupling scheme can be more clearly seen if we also consider the nonresonant transition (10). In Table II, the QC branching ratios of process (10) to process (3) obtained with the two decoupling schemes are shown along with the QM ratios. The QC ratios with the trajectory-based scheme show a reasonable agreement with the QM ratios. However, the coordinate-based scheme predicts the ratios to be very large as compared to the accurate QM ones. This seems to be a clear indication that the coordinate-based scheme is not adequate to describe processes involving resonance effects. Figures 3, 4, and 5 also exhibit QM results, which indicate that

the QC approach with the trajectory-based decoupling scheme reproduces the resonance peak structure reasonably well.

The QC peaks occur at $\lambda = 0.012$, shifted towards smaller values of λ from the QM peaks. At $\lambda = 0.012$, the potential difference $W_2 - W_1$ at the real parts of the branch points is equal to the vibrational energy separation 0.02; i.e., this λ fulfills the resonance condition at the branch points. Speaking in QM terms, at this λ , the two surfaces representing the initial and final quantum states cross at the real parts of branch points. (See related discussions in Sec. III. For our model, those points coincide with the points of the maximum nonadiabatic coupling.) Therefore, it is reasonable to expect the QC peaks to be at $\lambda = 0.012$ provided that the resonance effects are properly taken care of. That the QC peaks occur indeed at $\lambda = 0.012$ indicates that the resonance effects are incorporated in our QC method with the new decoupling scheme. The accuracy of the method, however, is limited by the assumption that the transition takes place only at branch points. This assumption is at least partly responsible for the inaccurate position of the QC peaks. Referring to Table I, we see that the agreement between the QC and the QM results on the position of the peaks is better at higher collision energies. We also note that the QC probabilities are in general somewhat larger than the QM probabilities. One might argue, however, that the inclusion of the Naitin factor⁹ will bring the QC probabilities down closer to the QM ones.

It is also interesting to note that interference effects, which are of course incorporated in the QM approach but suppressed in the QC, are not exhibited in the transition probability vs λ results. On the other hand, the absence of the interference effects in the QC method could be a part of the reason why the QC results become less accurate at lower collision energies.⁵

More stringent tests on the present decoupling scheme would seem to rest on its application to very low collision energies, perhaps even to cases where the collision energy is much lower than the resonance energy exchanged. However, it is debatable whether such a condition is a *sine qua non* for resonance considerations. The collision energies we have chosen are, in fact, lower than or, at worst, comparable to the vibrational quantum exchanged, near the real parts of the branch point, even though they may be large in other regions. Moreover, our exact quantum mechanical results also indicate that resonance effects do persist to the range of collision energies considered here, even though these effects tend to decrease as the collision energy increases. (The single-peak structure of the resonant P vs λ curve recurs through high E ; and the typical branching ratio for resonant to nonresonant transitions is ~ 10 at the peak value of λ , for $E = 0.035$.) Unfortunately the application of our present trajectory-based decoupling scheme is restricted to cases having a well-defined real velocity at the real parts of the branch point, which is not likely to be the case for very low collision energies.

APPENDIX: TRANSFORMATION OF COORDINATES

In terms of the new coordinates η and ξ defined by Eqs. (20), the kinetic energy can be written as¹²

$$T = \frac{1}{2} \dot{M} R^2 + \frac{1}{2} m \dot{r}^2 = \frac{1}{2} \mu_\eta \dot{\eta}^2 + \frac{1}{2} \mu_\xi \dot{\xi}^2 + \frac{1}{2} \mu \dot{\eta} \dot{\xi} . \quad (\text{A1})$$

Note that there exists a cross term containing $\dot{\eta} \dot{\xi}$ because the coordinates η and ξ are not separable in general. Substituting Eqs. (20) into Eq. (A1) and equating the terms that have the same powers of \dot{R} and \dot{r} , we obtain

$$M = \mu_\eta + \mu_\xi + \mu , \quad (\text{A2})$$

$$m = \mu_\eta \beta^2 + \mu_\xi / \beta^2 - \mu , \quad (\text{A3})$$

$$0 = -2\mu_\eta \beta + 2\mu_\xi / \beta + \mu(1/\beta - \beta) . \quad (\text{A4})$$

Solving Eqs. (A2)–(A4) for μ_η , μ_ξ , and μ , we obtain

$$\mu_\eta = (M/\beta^2 + m)/(\beta + 1/\beta)^2 , \quad (\text{A5})$$

which is Eq. (26) in Sec. IV,

$$\mu_\xi = (M/\beta^2 + m)/(\beta + 1/\beta)^2 , \quad (\text{A6})$$

and

$$\mu = (2M - 2m)/(\beta + 1/\beta)^2 . \quad (\text{A7})$$

Now if the system moves under the constraint that $\dot{\xi}$ remains zero, then

$$T = \frac{1}{2} \mu_\eta \dot{\eta}^2 = P_\eta^2 / 2\mu_\eta , \quad (\text{A8})$$

and

$$k_\eta = P_\eta / \hbar = (2\mu_\eta T)^{1/2} / \hbar = [2\mu_\eta (E - W)]^{1/2} / \hbar , \quad (\text{A9})$$

where W is the potential energy.

¹For a review of the theory of nonadiabatic collision processes, see J. C. Tully, in *Dynamics of Molecular Collisions*, Modern Theoretical Chemistry, edited by W. H. Miller (Plenum, New York, 1976), Part B, p. 217.

²Since we consider nonadiabatic processes throughout this paper, we will be using the term "QC method" to mean the extension of the usual QC method to account for nonadiabatic transitions, i.e., by QC method, we actually mean the surface-hopping trajectory method [J. C. Tully and R. K. Preston, *J. Chem. Phys.* **55**, 562 (1971)] or its variations.

³A. Komornicki, T. F. George, and K. Morokuma, *J. Chem. Phys.* **65**, 48 (1976).

⁴I. H. Zimmerman and T. F. George, *Chem. Phys.* **7**, 323 (1975).

⁵W. H. Miller, *J. Chem. Phys.* **68**, 4431 (1978).

⁶J. C. Tully, *J. Chem. Phys.* **59**, 5122 (1973).

⁷T. E. Sharp and D. Rapp, *J. Chem. Phys.* **43**, 1233 (1965).

⁸J. C. Light and R. B. Walker, *J. Chem. Phys.* **65**, 4272 (1976).

⁹J. R. Laing, T. F. George, I. H. Zimmerman, and Y. W. Lin, *J. Chem. Phys.* **63**, 842 (1975).

¹⁰D. L. Bunker, *Meth. Comp. Phys.* **10**, 287 (1971).

¹¹R. N. Porter and L. M. Raff, in *Dynamics of Molecular Collisions*, Modern Theoretical Chemistry, edited by W. H. Miller (Plenum, New York, 1976), Part B, p. 1.

¹²In this Appendix, the discussion is presented without reference to any particular point or trajectory. The subscript Q is therefore dropped.

APPENDIX C

Pulsed Visible Chemiluminescence Experiments

M. D. Burrows and D. J. Benard

Introduction

In order to achieve lasing on an electronic transition in a typical diatomic molecule it is necessary to rapidly generate a copious supply of molecules in the upper level of the laser transition. At shorter wavelengths this requirement becomes more difficult to satisfy because of rapidly decreasing stimulated emission cross-sections. Further, when a chemical reaction scheme is employed as the source of excitation it is also necessary to hold down the reagent concentrations in order to prevent quenching of the lasing species by the reagent or product molecules. Therefore, it is requisite in such cases to carry out the chemical reactions in as rapid a way as possible in order to obtain the necessary pump rate.

Traditionally, chemical lasers have been of the mixing type and have employed reactions that initiate spontaneously as mixing occurs. This approach is most appropriate to the generation of CW lasers, however, since the mixing is limited by diffusion which often proceeds slowly compared to gas kinetic reaction rates, it may be difficult to achieve lasing on diatomics at shorter wavelengths using this scheme. As an

alternative, we have considered laser schemes based on gas phase chemiluminescence reactions that do not initiate spontaneously but proceed via a branched chain reaction kinetics. This feature not only allows premixing of the reagents but also provides a chemical amplifier effect which allows one to "trigger" the reaction by a relatively small input of optical or electrical energy which produces the initial chain carrier species. The resultant laser action would therefore be pulsed, which may be advantageous in itself. Enhanced propagation and target effects have been demonstrated for repetitively pulsed DF chemical lasers relative to their CW counterparts; however, it remains to be seen what significant advantages may accrue for pulsed visible lasers.

Experimental Method

Fig. 1 shows the experimental apparatus. Chlorine dioxide (ClO_2) is generated by passing Cl_2 gas over NaClO_2 crystals. (Ref. 1) The ClO_2 is collected in a cold trap prior to loading into the reaction cell. A fuel species, typically acetylene (C_2H_2) is then added to the reaction cell and is allowed to mix with the chlorine dioxide. A single 10 mJ, 20 nsec pulse of 3500 Å light from a XcF excimer laser is then used to detonate the mixture. The absorption coefficient of ClO_2 at 3500 Å is so high (3000 l/mole-cm) that the 10 mJ pulse is almost totally absorbed after traversing less than 1 cm of ClO_2 at partial pressures on the order of 50 Torr. Irradiation of ClO_2 at this wavelength yields predissociation into $\text{ClO} + \text{O}$, which is probably followed by the rapid (10^{-11} cm³/molecule-sec) exothermic reaction $\text{ClO} + \text{O} \rightarrow \text{Cl} + \text{O}_2^*$. (Ref. 2) The initial UV laser

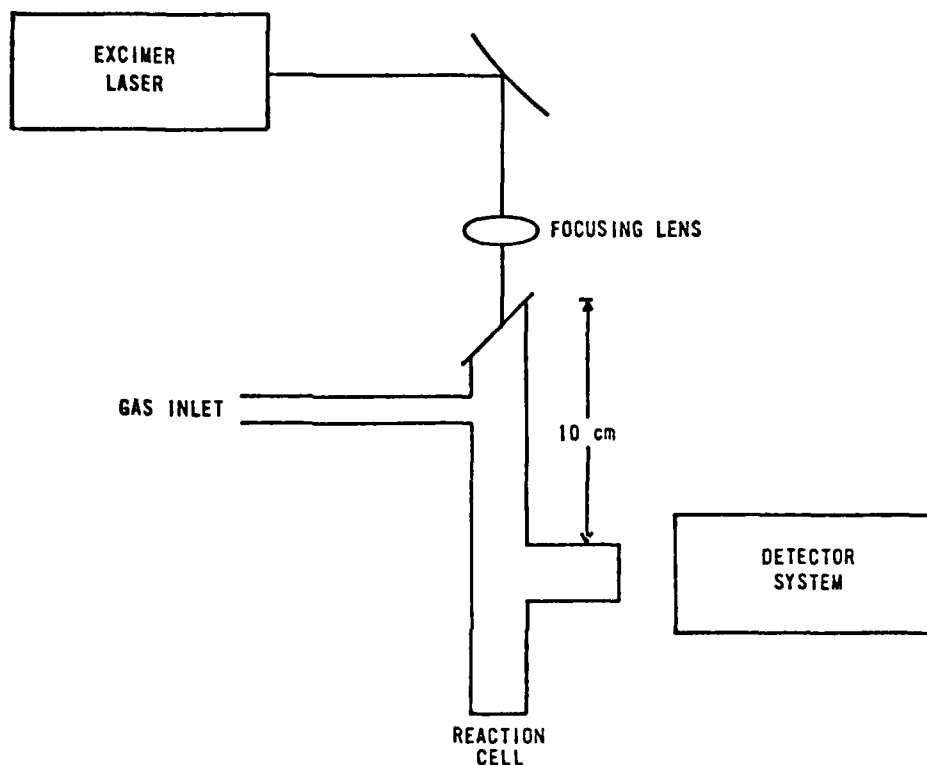


Fig. 1. Experimental apparatus for pulsed chemiluminescence experiments. The excimer laser can be operated at 3500 \AA (XeF), 2940 \AA (KrF), or 1930 \AA (ArF). The detector consists of either an interference filter and photomultiplier tube or a grating monochromator and optical multichannel analyzer system. The quantum efficiency of the optical multichannel analyzer is 10%, decreasing to zero at the sensitivity limits of 3500 \AA and 8400 \AA . The resolution is 5 \AA per channel with a memory capacity of 860 counts for each channel.

pulse, therefore, produces high densities of ClO , O , Cl , and excited O_2 in a small volume which then chemically ignites the remaining ClO_2 and fuel (C_2H_2). The detector in Fig. 1 consists of either a photomultiplier tube and interference filter for intensity versus time profiles or a grating monochromator and optical multichannel analyzer system to record single detonation spectra. The observation side-arm is deliberately located a distance away from the end window so that optical pumping by the XeF laser is not observed. Typical partial pressures are 150 Torr of ClO_2 and 75 to 100 Torr of C_2H_2 . Soot formation on the cell windows becomes a problem if higher C_2H_2 pressures are used.

Results

The detonation of ClO_2 and C_2H_2 mixtures resulted in an intense blue-green chemiluminescence. A typical spectrum of the chemiluminescence is shown in Fig. 2. The observed chemluminescence is easily identified as the $\text{C}_2(d^3\pi \rightarrow a^3\pi)$ Swan bands. (Ref. 3, 4) The emission is very intense and requires the use of neutral density filters in order to prevent saturation of the optical multichannel analyzer detector.

Excitation of the Swan system can also be obtained by detonation of $\text{HN}_3 + \text{C}_2\text{H}_2 + \text{N}_2\text{O} + \text{He}$ mixtures using a single 30 mJ, 20 nsec pulse of 2490 Å KrF excimer laser light. As Fig. 3 shows, strong CN Violet band emission is also observed from this mixture. Excitation of the Swan band system by such mixtures depends much more critically on relative reactant concentrations, but produces a much "cleaner" and better developed C_2 Swan system

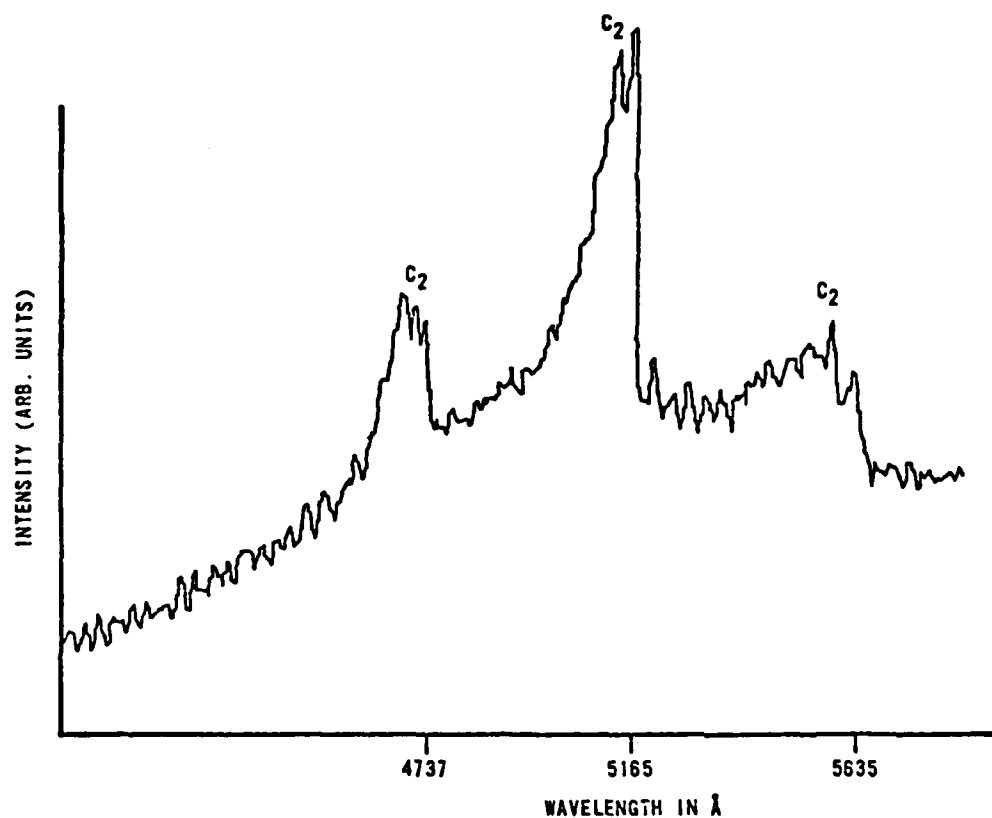


Fig. 2. Chemiluminescence spectrum from the detonation of a mixture of 150 Torr ClO_2 plus 90 Torr C_2H_2 . The violet band heads at 5635, 5165, and 4737 Å are the C_2 Swan bands ($d^3\pi \rightarrow a^3\pi$). The detonation was initiated using a single 3500 Å excimer laser pulse and the spectrum acquired using the optical multichannel analyzer system and a neutral density filter of 3.

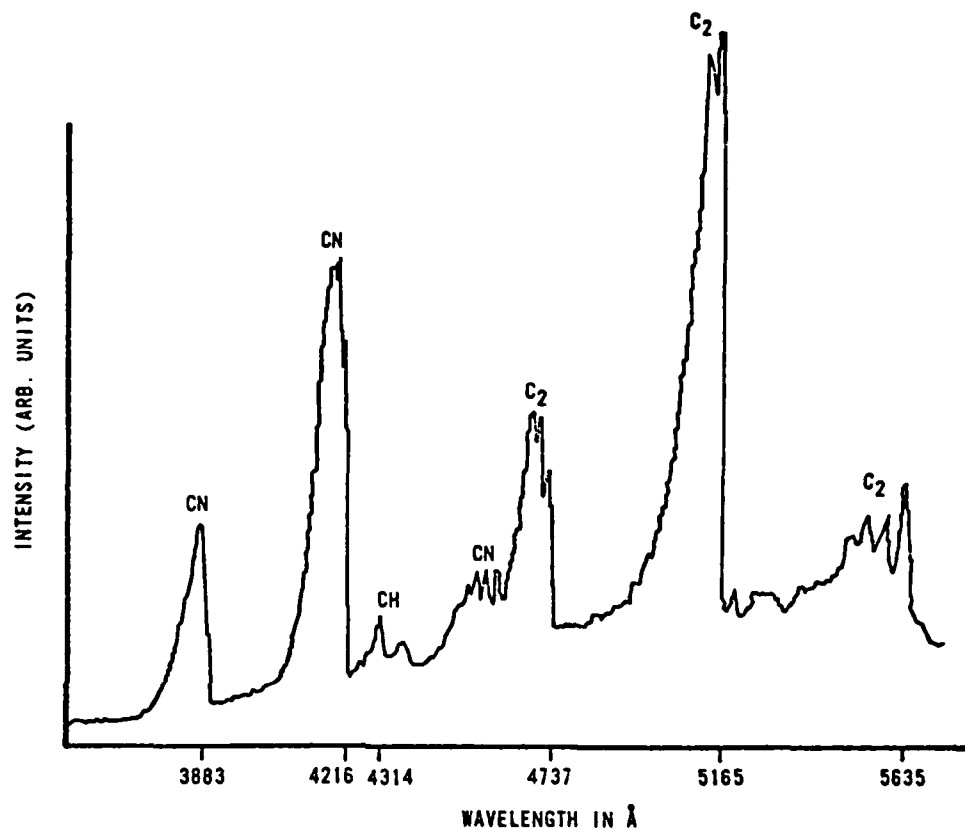


Fig. 3. Chemiluminescence spectrum from the detonation of a mixture of 150 Torr HN_3 + 50 Torr C_2H_2 + 50 Torr N_2O + 200 Torr He acquired using the optical multichannel analyzer system and a neutral density filter of 2. The intense violet degraded band heads at 5635, 5165, and 4737 Å are the C_2 Swan bands, while the violet degraded band heads at 4578, 4216, and 3883 Å are the CN violet bands ($\text{B}^2\Sigma \rightarrow \text{X}^2\Sigma$). The weak violet degraded head at 4314 Å is due to the CH radical $\text{A}^2\Delta \rightarrow \text{X}^2\Pi$ transition.

than does the detonation of ClO_2 and C_2H_2 mixtures, where the Swan bands are superimposed on a strong background of continuum emission. Detonation of mixtures containing only HN_3 and C_2H_2 produces weak Swan bands, while the addition of He buffer gas enhances the Swan band emission. The Swan band intensity is increased further by using both He and N_2O . The detonation chemistry of HN_3 and C_2H_2 mixtures appears to be strongly dependent on trace impurities in the He buffer gas, since replacing He with Ar completely removes both the CN and C_2 emission. Previous researchers have found using isotopic substitution that the carbon-carbon bond is definitely broken in reactions producing C_2 , (Refs. 5, 6) which is consistent with the observation in the present experiments of excited CH radicals ($A^2\Delta \rightarrow X^2\pi$ transition at 4314 \AA) when mixtures of $\text{HN}_3 + \text{C}_2\text{H}_2 + \text{N}_2\text{O} + \text{He}$ are detonated by KrF laser light.

The temporal behavior of the chemiluminescence pulses from detonation of ClO_2 and C_2H_2 mixtures was monitored by replacing the OMA with a photomultiplier tube and 5100 \AA interference filter. A typical time history is shown in Fig. 4. The risetime of the pulse is typically 30-50 μsec , while the "burn-time" exceeds 1 msec. The time delay before the rapid onset of light emission is on the order of the time required for a shock front to travel from the laser input window to the side-arm where light emission is observed.

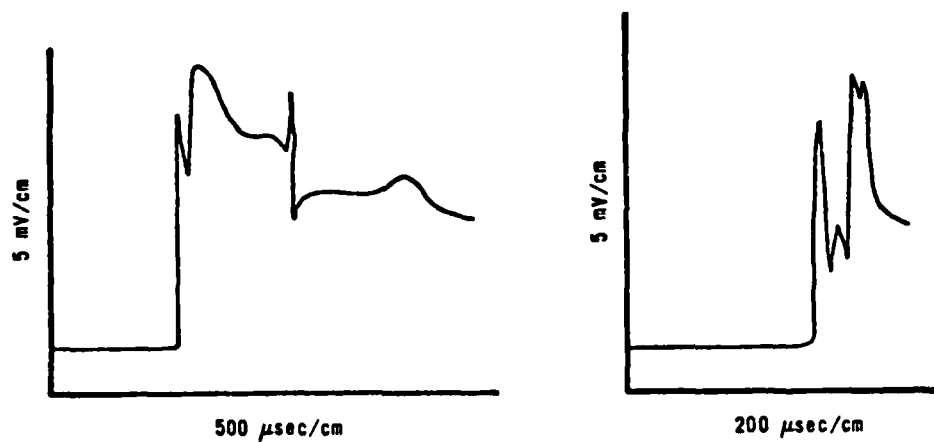


Fig. 4. Time history of emission from detonation of mixtures of 50 Torr ClO_2 and 50 Torr C_2H_2 using a 5100 Å interference filter and photomultiplier tube.

Discussion

The C_2 Swan bands are commonly seen in hydrocarbon flames at atmospheric pressure. (Ref. 7). The $d^3\pi \rightarrow a^3\pi$ transitions are highly vertical and thus appear in a characteristic $\Delta v=0$ vibrational sequence with the (0,0) band head at 5165 Å. Contributions from higher vibrational levels appear at shorter wavelengths spaced by $\omega_e \sim 1800 \text{ cm}^{-1}$. (Ref. 4) Experiments with C_2H_2 in flames have shown that C_2 Swan band emission is many orders of magnitude more intense than can be predicted on the basis of the adiabatic flame temperature and statistical (Boltzman) population distributions (Ref. 8) Therefore one may infer that the $C_2(d^3\pi)$ state is specifically populated by chemical reactions in flames. Further, cavity resonance experiments have failed to show any measureable absorption in moderate pressure flames (Ref. 9) from which one might surmise that $C_2(a^3\pi)$ is removed via a chemical process since statistically the $C_2(a^3\pi)$ state should be thermally populated. The radiative lifetime of the $C_2(a^3\pi)$ state is on the order of 200 nsec. (Ref. 10) so it seems probable that rapid chemical removal of $C_2(a^3\pi)$ at our $10^{19}/\text{cm}^3$ concentrations could sustain an inversion. These results taken in conjunction with our experimental observations support the possibility of producing a pulsed visible chemical laser on the C_2 Swan bands in premixed ClO_2 and C_2H_2 mixtures.

At this time the mechanism of reaction is unknown, thus it is impossible to speculate in any detail regarding the kinetics of the reaction. The simplest interpretation of Fig. 4 (time history of chemiluminescence) is

that the initial rise and the associated high frequency structure results from a chemically driven shock wave that is followed by uniform burning of the reagents behind the shock front which persist until the reactants are depleted. Thus the chemiluminescence is actually a quasi CW process since the reaction time is long compared to the radiative decay rate. One would estimate that a limiting rate of $\sim 10^{-13}$ cm³/molecule-sec controls the chemiluminescence process based on the reagent concentration and the chemiluminescence decay rate.

Of course whether a chemically pumped C₂ laser is possible will depend critically on the details of the kinetics, however, one may show that if the kinetics efficiently produce C₂(d³π) and selectively destroy C₂(a³π) that gain coefficients on the order of 1/cm can be easily generated by reacting a 200 Torr mixture of ClO₂ and C₂H₂ in 10⁻³ sec. At such densities the chemical energy is stored at the rate of ~ 1 KJ/liter assuming efficient production and extraction of the chemical energy as laser photons. A theoretical specific energy in excess of 1MJ/lb is calculated by dividing the photon energy by the mass of the reagent species. In practice it is unlikely, however, that such optimistic figures will actually be obtained; however as a result of the thermal expansion attendant with the reactive heat release it would appear that atmospheric pressure recovery is feasible in a ramjet configuration.

Summary

We have shown that by premixing reagents and pulsing a chemiluminescent reaction that one may overcome some of the difficulties inherent to the

production of a visible chemical laser operable on a diatomic species. The reaction of ClO_2 and C_2H_2 is one such reaction that produces electronically excited C_2 molecules with properties appropriate to laser action on the $d^3\pi \rightarrow a^3\pi$ transitions, given kinetics that favor inversion. Such lasers in a pulsed mode are capable of achieving high gain coefficients and are characterized by high specific energy and high energy storage per unit volume in the laser cavity.

REFERENCES

1. R.D. Stuart, D.R. Snelling, K.D. Foster, and R. Lambert, "Purely Chemical Laser Based on Chlorine Atom Reactions: ClO_2 Generator", DREV Rep. 4005/76, Apr 1976.
2. P.P. Bemand, M.A.A. Clyne, and R.T. Watson, JCS Far, Trans. I 69, 1356 (1976)
3. K.P. Huber and G. Herzberg, Molecular Spectra and Molecular Structures, IV Constants of Diatomic Molecules, Van Nostrand Reinhold Co., NY 1979.
4. B. Rosen, Spectroscopic Data Related to Diatomic Molecules, Pergamon, NY 1970.
5. A.R. Fairbairn, Proc. Roy. Soc. 267, 88 (1962).
6. R.E. Ferguson, J. Chem. Phys. 23, 2085 (1955).
7. A.G. Gaydon, The Spectroscopy of Flames, Chapman and Hall, London 1974.
8. R. Bleekrode and W. C. Nieupoort, J. Chem. Phys., 43, 369 (1965).
9. M. Steinberg, private communication based on work at University of California Quantum Institute, Santa Barbara, CA under ARPA contract DAAH01-75-C-0039, 1976.
10. Smith, Astrophysical Journal 156, 791 (1969).

